Salt and Pepper Noise Removal from a Digital Image Using a New Approach Based on Fuzzy Cellular Automata and Anfis

Mohammad Mehdi Piroozmandan [*1], Fardad Farokhi [2], Mohammad Ali Piroozmandan [3]

[1] Department of Computer Engineering, Shiraz Branch, Islamic Azad University, Shiraz, Iran, moh.piroozmandan.eng@iauctb.ac.ir
2 Department of Biomedical Engineering, Central Tehran Branch, Islamic Azad University, Tehran, Iran, f_farokhi@iauctb.ac.ir
[3] Department of Geology, Shiraz Branch, Islamic Azad University, Shiraz, Iran, m.piroozmandan@iaushiraz.ac.ir

Abstract

This paper proposes a novel method for restoring images corrupted by impulse noise. This new method is based on fuzzy cellular automata and an adaptive neural fuzzy inference system (Anfis). The proposed method consists of two phases: identifying and removing salt and pepper noise. In the first phase of the method proposed, salt and pepper noise pixels are identified in two steps. In the first step of the first phase, salt and pepper noises are detected by the average and minimum values of the pixels in the neighborhood of the center pixel. In order to improve the accurate rate of noise detection, pixels that are not detected as noise are re-evaluated by a new algorithm in the second step of the first phase. This new algorithm uses the measure of cosine similarity of Moore's neighborhood values around the central cell, which is based on four types of pixel placement patterns. The state of the pixels is re-evaluated by the fuzzy cellular automata. In the second phase of the proposed method, noisy pixels are restored using Anfis based on Moore neighborhood pixels around the central cell. The method proposed in this paper is evaluated using PSNR and SSIM. Also, the quantitative and qualitative results show that the new method proposed in this paper is robust in different noise levels from 10% to 90%, and image details such as edges are preserved better compared to other filters.

Keywords: Cellular Automata, Fuzzy Cellular Automata, Anfis , noise detection, de-noising
Article history: Received 2024/05/31; Revised 2023/06/15; Accepted 2024/07/12, Article Type: Research paper

https://doi.org/10.82234/ijsee.2024.1121383

1. Introduction

The main goal of image processing science is to obtain the information required for use in specific applications in various engineering and medical sciences. The effective removal of noise from digital images is of particular importance because the implementation of image processing tasks such as compression, edge detection, and image segmentation strongly depend on the results of the noise removal operation [1-2, 33-35].

Since pictures are usually taken with non-ideal devices, it is possible that due to improper functioning of some parts of the camera, such as the lens, and even shaking of the photographer's hand, these pictures may be damaged during the taking. In the stages of transfer and storage of images, the quality of images may decrease due to factors such as noise channels and environmental factors [2]. Considering that this low quality of the images lowers the performance of the processing process and may lead to incorrect decisions. Image enhancement, and image restoration are the most critical topics in image processing that remove noises and improve image quality. Image enhancement includes methods that try to restore the image without knowing the image damage model, but image restoration includes objective methods that try to improve the image by knowing the image damage model. There are different types of noise in digital images, and the two most common types are Impulse noise and Gaussian noise. Images are often corrupted by noise for various reasons, such as faults in camera sensors during recording, transmission exceptions and errors during communication, and other errors in processing. Impulse noise, even at low percentages, can significantly change image resolution. Impulse noise includes salt and pepper noise (SP) and random value noise (RVN), which severely damages the structures and contents of the

image and severely reduces its quality [2-3]. An image containing impulse noise can be described as follows:

$$S_{i,j} = \begin{cases} n_{i,j} & with\ probability \quad p \\ f_{i,j} & with\ probability \quad 1-p \end{cases} \tag{1}$$

Where $S_{i,j}$ denotes a noisy image pixel and $f_{i,j}$ denotes a noise free image pixel at the location (i,j). Also, $n_{i,j} \in [L_{min}, L_{max}]$ is a noisy impulse at the location (i,j). Where L_{min} and L_{max} denote the lowest and the highest pixel luminance values within the dynamic range, respectively. The simplest and most frequently used impulse noise model is the salt-and-pepper noise, where noisy pixels take either minimal or maximal value, i.e., $n_{i,j} \in \{L_{min}, L_{max}\}$. If F(x,y) is a noise-free 8-bit image and this image is corrupted by salt-and-pepper noise, the noise pixels can have only two maximum and minimum values in the dynamic range and can be seen as white or black dots in the image.

2. Related works

In this section, we review some studies related to our work that focus on the noise detectors and filters design for impulse noise (IN) removal. The standard median filter is a classical non-linear filtering technique to remove impulse noise by the median pixel from the sorted pixels of a given working window [4]. This filter replaces the central pixel value with the median value of its neighboring pixels. Also, a variety of advanced median filter methods and filters have been presented, such as central weighted median filter [5], vector switching median filter [6], adaptive window length recursive median filter [7], and adaptive switching median filter [8]. These methods are simple, and when the impulse noise density in the image is low, they perform well to remove the noise. However, when the noise density in the image is high, they do not perform well, and the restored image becomes blurry.

Filters and methods such as Center-Weighted Median Filter (CWMF) [9], Adaptive Median Filter (AMF) [10], and Adaptive Center Weighted Median (ACWM) filter [11] and recursive weighted median filter [12], are nonlinear and are also variations of the median filter.

In [13–15, 39-41] techniques are based on an Adaptive Neuro-Fuzzy Inference System (ANFIS) for impulse noise removal from corrupted images. Also, other different techniques such as noise adaptive fuzzy switched median (NAFSM) [16] have been widely applied to color image denoising [17–18]. These methods are good at detecting noises when the noise density is high but have some disadvantages. When in digital images the density is high, these methods include computational complexity and important image details might not be recovered and even some image edges might be deleted.

Also, many methods have been suggested for salt and pepper denoising [14,42-48]. Given that corrupted pixels by SAP noise are the maximum or minimum values of noisy images, median-based filter approaches have received considerable attention as the starting point of the efforts to remove SAP noise. The different applied median filter (DAMF) uses two consecutive median filters [42]. In contrast to DAMF, the adaptive Cesáro mean filter (ACmF) [47] employs the Cesáro mean instead of the median in a recursive algorithm, improving performance but increasing the execution time. In [48], a four-stage median-average (FoMA) algorithm is introduced, employing four-step median and mean filters.

This paper presents a new method based on cellular automata and Anfis network, consisting of three new algorithms. This method consists of two phases. In the first phase, two new algorithms identify damaged pixels in the digital image in two steps. In other words, in the first stage of the first phase, the maximum, minimum, and average values of the pixels in the neighborhood of the central pixel are calculated by the first algorithm. Then, the salt and pepper noise pixels are identified. In order to improve the accuracy in identifying the damaged pixels in this phase, the pixels that are not detected as noise are evaluated again by another new algorithm (the second algorithm). This new algorithm uses the cosine similarity measure of the central cell's Moore's neighborhood values by four types of pixel placement patterns in Moore's neighborhood, and the noise or non-noise of the pixels is checked again by cell automata. In the second phase of the proposed method, the impulse noise pixels are restored using Anfis based on the neighboring pixels of the centeral cell.

3. Cellular automata

Cellular automata or CA are discrete dynamical systems whose behavior is based on local relations and can be used to simulate different systems. The cellular automata can be used to model many diverse phenomena so that in computational science application areas such as image processing, can be used as an effective tool [19-21]. The rules in cellular automata are local and uniform so that each cell obtains its new state by considering its neighbors. Also, time is discrete in cellular computers, and calculations are done in parallel [1-2,19]. Localization means that in determining the new value of each cell, the adjacent cells are affected, and the more distant cells do not influence the new value of each cell. Cells at each time step (t

=0, 1, 2, …, n) follow a local transition function and according to their current state and their neighbors, move to a new structure. In other words, the next position of a cell is locally determined by the current position of that cell and the current position of its neighboring cells. In cellular automata, cells can take many different positions. So cellular automata can be presented in one-dimensional, two-dimensional, or multidimensional models (M-D CA) so that one-dimensional cellular automata are the simplest model of cellular automata. Cellular automata can be defined by four tuples {L, Q, r, F}, where "L" is the regular grid of cells, "Q" a finite set of states, "r" and "F" are neighborhood radius and transition function. Different Types of neighborhood structures are used for cellular automata, Von Neumann, and Moore neighborhood structures are most commonly used (see Fig. 1). The Von Neumann and Moore neighborhood of radius r =1 is as shown in Eq. (1) [19-21].

$$x_{(i,j)} = \{(i',j')\epsilon L \mid |i'-i| + |j'-j| \leq 1\}$$
$$x_{(i,j)} = \{(i',j')\epsilon L \mid |i'-i| \wedge |j'-j| \leq 1\} \quad (2)$$

Where, L is a regular lattice (the elements of L being called cells), N is a finite set of neighborhood indices such that ∀r∈L. In Von Neumann's neighborhood Cellular Automata, shown in Figure (1) each cell changes its position according to the positions of the upper, lower, left, and right neighbor cells as well as the cell itself. But in Moore's neighborhood, four diagonal cells have been added to the neighborhood. In Fig. 2, the central cell $x_{i,j}$and its eight surrounding neighbors are shown in the neighboring structure of two-dimensional cellular automata. In two-dimensional cellular automata, the cell status at time t+1 is updated based on the transfer function F and the cell status at time t. The following relation shows the cell status at time t+1 in two-dimensional cellular automata:

$$x_{(i,j)}^{(t+1)} = F(x_{(i+1,j)}^{(t)}, x_{(i+1,j-1)}^{(t)}, x_{(i,j-1)}^{(t)}, x_{(i-1,j-1)}^{(t)}, x_{(i-1,j)}^{(t)}, x_{(i-1,j+1)}^{(t)}, x_{(i,j+1)}^{(t)}, x_{(i+1,j+1)}^{(t)}) \quad (3)$$

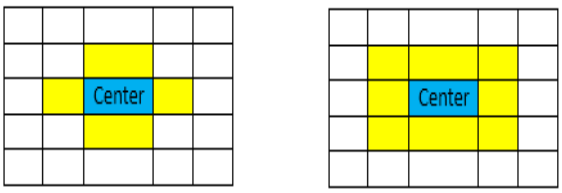

Fig. 1. Van Neumann neighborhood model and Moore neighborhood model

$x_{i-1,j-1}$	$x_{i-1,j}$	$x_{i-1,j+1}$
$x_{i,j-1}$	$x_{i,j}$	$x_{i,j+1}$
$x_{i+1,j-1}$	$x_{i+1,j}$	$x_{i+1,j+1}$

Fig. 2. The position of the central pixel in the 3×3 window

Fuzzy logic is one of the powerful tools in artificial intelligence so that it can be used effectively in processing uncertain and implicit data. Another powerful tool called fuzzy cellular automata (FCA) has been introduced in [23]. In this structure, fuzzy values are used instead of definite values for cell states and traction functions. Cell states are in the form of linguistic variables. In [22, 24], Cellular Automata has been used with the help of fuzzy logic to remove the noise of the image, so in the proposed method a new fuzzy logic-based local transmission function is proposed which removes the impulse noise of the image. Also, for example, in [25] a new filter is introduced that detects impulse noise in the image using statistical information and removes it based on cellular automata and fuzzy logic. In this study, it is shown that cellular automata and fuzzy cellular automata are effective and powerful tools in image noise removal.

4. The adaptive neural-fuzzy inference system (ANFIS)

Adaptive neural-fuzzy inference system called ANFIS is implemented based on adaptive networks [26-28,41]. The ANFIS [29,30,41] is a multilayer feed-forward network, which uses neural network learning algorithms and fuzzy reasoning to map an input space to a target output. In fact, Anfis is a basis for creating a set of if-then-else rules that are defined with appropriate membership functions for generating input-output pairs. Anfis is a multilayer feed-forward network in the form of a five-layer network, the Anfis structure is shown in Figure (3).

This figure shows that this network has two inputs (x,y) and one output g. Here, (g) and (x, y) denote the intensity gray values of the pixels and the spatial positions, respectively. Each input of the ANFIS structure has two different triangular membership functions and the rule base contains a total of 4 rules, which are detailed as follows:

- *Rule 1: if x is* A_1 *and y is* B_1 *then* $f_{11} = p_{11}x + q_{11}y + 1$
- *Rule 2: if x is* A_1 *and y is* B_2 *then* $f_{12} = p_{12}x + q_{12}y + 1$
- *Rule 3: if x is* A_2 *and y is* B_1 *then* $f_{21} = p_{21}x + q_{21}y + 1$
- *Rule 4: if x is* A_2 *and y is* B_2 *then* $f_{22} = p_{22}x + q_{22}y + 1$

Where p, q and r denote the consequent parameters [27]. Also, a combination of least-squares and back-propagation gradient descent method has been used at the training phase of the fuzzy structure.

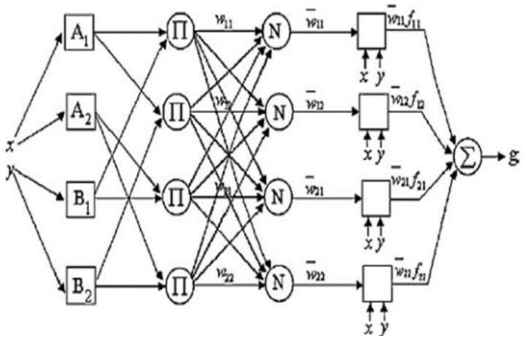

Fig. 3. Anfis fuzzy neural network structure

Let the membership functions of fuzzy sets A_i and B_j , be μ_{A_i} and μ_{B_i}respectively, where i = 1,2, and j = 1,2. Then, the five layers of the ANFIS structure are defined as follows.

$$\mu_{A_i}(x) = \max\left(min\left(\frac{x-a_i}{b_i-a_i}, \frac{c_i-x}{c_i-b_i}\right), 0\right) \quad (4)$$

$$\mu_{B_j}(y) = \max\left(min\left(\frac{y-a_j}{b_j-a_j}, \frac{c_j-y}{c_j-b_j}\right), 0\right) \quad (5)$$

Where $\mu_{A_i}(x)$ and $\mu_{B_j}(y)$ were chosen as triangular membership functions with the parameters of a, b and c [27].

$$\omega_{ij} = \mu_{A_i}(x)\mu_{B_j}(y) \quad (6)$$

Where ω_{ij}denotes the logical operation and which has been used as product for all the rules [27].

$$\bar{\omega}_{ij} = \frac{\omega_{ij}}{\omega_{11}+\omega_{12}+\omega_{21}+\omega_{22}} \quad (7)$$

Where $\bar{\omega}_{ij}$ is the normalized value of ω_{ij}.

Every node in this layer is a square node with a linear function [27] η_{ij} as

$$\eta_{ij} = \bar{\omega}_{ij} f_{ij} = \bar{\omega}_{ij}(p_{ij}x + q_{ij}y + r_{ij}) \quad (8)$$

The single node in this layer is labeled with Σ, which computes the overall output, g, as the summation of all incoming signals, i.e.

$$g = \sum_{i=1}^{2}\sum_{j=1}^{2}\eta_{ij} \quad (9)$$

5. Proposed method

The proposed method includes two phases. In the first phase, in two steps, corrupted pixels are identified by new algorithms. In the second phase of the proposed method, the pixels detected as impulse noise are restored using Anfis based on the neighbouring pixels of the central cell. The phases presented in the proposed method are as follows:

A) First phase

In this step, the impulse noise pixels in the digital image are identified by two steps. In the first step of the first phase, a window with dimensions of 3×3 is scanned on the image. Then, impulse noises are identified by the following algorithm:

Algorithm 1:

- The average of 8 pixels around the central pixel is calculated as follows in Figure 2, and then we go to step 2 (the N value shows the number of neighbouring pixels around the central pixel):

$$x_{average} = \frac{1}{N}\sum (x_{i-1,j-1}, x_{i-1,j}, x_{i-1,j+1}, x_{i,j-1}, x_{i,j+1}, x_{i+1,j-1}, x_{i+1,j}, x_{i+1,j+1}) \quad (10)$$

- The minimum of 8 pixels around the central pixel is calculated as shown in Figure 2 as follows, and then we go to step 3:

$$x_{min} = \min(x_{i-1,j-1}, x_{i-1,j}, x_{i-1,j+1}, x_{i,j-1}, x_{i,j+1}, x_{i+1,j-1}, x_{i+1,j}, x_{i+1,j+1}) \quad (11)$$

- If (x_{min}=$x_{average}$ and $x_{i,j}$=0) or (x_{min}=$x_{average}$ and $x_{i,j}$=255) then the central pixel $x_{i,j}$ is the corrupted pixel else go to step 4.
- If ($x_{min} \le x_{i,j} < x_{average}$) then the central pixel $x_{i,j}$is the corrupted pixel else $x_{i,j}$ is considered as the uncorrupted pixel.

At first step, detected pixels may be uncorrupted pixels. So, in order to improve accurate rate of noise detection, the first detection pixels are judged again by algorithm 2:

Algorithm 2:

- If x_{min}=0 or $x_{average}$=0 or x_{min}=255 or $x_{average}$=255 then go to step 3, else go to step2.
- We calculate the Euclidean distance of the central pixel (as shown in Figure 2) from 8 pixels around the central pixel as in the following equation, and then go to step 3:

$$d_i = \left|x_{i,j} - x_{i+v,j+u}\right|, (v,u) \in \{-1,0,1\} \quad (12)$$

- We calculate the average and standard division like the following relations and then we go to step 4 (the value of N is equal to 8):

$$x_{avg} = \frac{1}{N}\sum (x_{i-1,j-1}, x_{i-1,j}, x_{i-1,j+1}, x_{i,j-1}, x_{i,j+1}, x_{i+1,j-1}, x_{i+1,j}, x_{i+1,j+1}) \quad (13)$$

$$ST = \sqrt{\frac{1}{N-1}\sum (d_i - x_{avg}} \quad (14)$$

- Corrupted pixels are identified using cellular automata by the following relationship:

$$x_{i,j} = \begin{cases} x_{i,j} \text{ is a corrupted pixel}, F(i,j) = \frac{x_{avg}}{ST} \ge \alpha \\ x_{i,j} \text{ is a uncorrupted pixel}, F(i,j) = \frac{x_{avg}}{ST} < \alpha \end{cases} \quad (15)$$

- The value of α is determined by the following equation (the value of N is equal to 8):

$$\alpha = \left(1 - \frac{1}{N}\right) ST \quad (16)$$

B) Second phase

In the section, after identifying and detecting the noisy pixels by the first phase of the proposed method, the second phase aims to restore the corrupted pixels by an adaptive neural fuzzy inference system (ANFIS). The restoration of the corrupted pixels is detailed as follows (Algorithm 3):

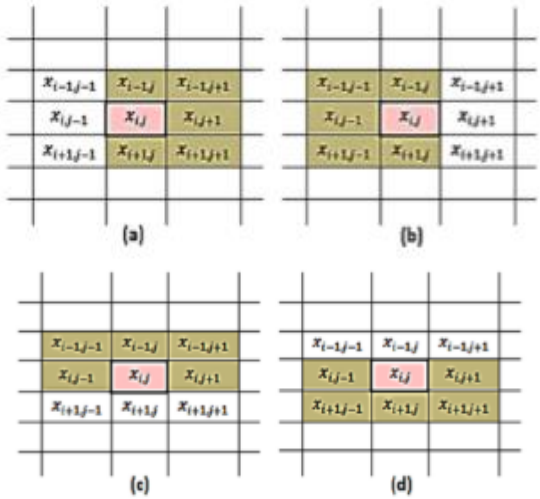

Fig. 4. Four different positions of the five neighboring pixels of the central pixel based on the models (a), (b), (c) and (d).

Algorithm 3:

- The following parameters are first set and quantified (see figure 4):

$$\overrightarrow{d_1} = (x_{i-1,j-1}, x_{i-1,j}, x_{i-1,j+1}, x_{i,j-1}, x_{i,j+1}) \quad (17)$$

$$\overrightarrow{d_2} = (x_{i,j-1}, x_{i+1,j-1}, x_{i+1,j}, x_{i+1,j+1}, x_{i,j+1}) \quad (18)$$

$$\overrightarrow{d_3} = (x_{i-1,j}, x_{i-1,j+1}, x_{i,j+1}, x_{i+1,j+1}, x_{i+1,j}) \quad (19)$$

$$\overrightarrow{d_4} = (x_{i-1,j-1}, x_{i-1,j}, x_{i,j-1}, x_{i+1,j-1}, x_{i+1,j}) \quad (20)$$

$$cos^{1}\alpha = \frac{\overrightarrow{d_1}.\overrightarrow{d_2}}{|\overrightarrow{d_1}||\overrightarrow{d_2}|} \quad (21)$$

- If $|\overrightarrow{d_1}| = 0$ or $|\overrightarrow{d_2}| = 0$ or $|\overrightarrow{d_3}| = 0$ or $|\overrightarrow{d_4}| = 0$ then go to step 4, else the following values will be calculated and go to step 3:

$$cos^{2}\alpha = \frac{\overrightarrow{d_1}.\overrightarrow{d_3}}{|\overrightarrow{d_1}||\overrightarrow{d_3}|} \quad (22)$$

$$cos^{3}\alpha = \frac{\overrightarrow{d_1}.\overrightarrow{d_4}}{|\overrightarrow{d_1}||\overrightarrow{d_4}|} \quad (23)$$

$$cos^{4}\alpha = \frac{\overrightarrow{d_2}.\overrightarrow{d_3}}{|\overrightarrow{d_2}||\overrightarrow{d_3}|} \quad (24)$$

$$cos^{5}\alpha = \frac{\overrightarrow{d_2}.\overrightarrow{d_4}}{|\overrightarrow{d_2}||\overrightarrow{d_4}|} \quad (25)$$

$$cos^{6}\alpha = \frac{\overrightarrow{d_3}.\overrightarrow{d_4}}{|\overrightarrow{d_3}||\overrightarrow{d_4}|} \quad (26)$$

- The maximum value $cos^{1}\alpha$, $cos^{2}\alpha$, $cos^{3}\alpha, cos^{4}\alpha, cos^{5}\alpha$ and $cos^{6}\alpha$ is calculated as (26) then go to step 4:

$$M^{max} = \max\begin{pmatrix}\cos^{1}\alpha, \cos^{2}\alpha, \cos^{3}\alpha, \cos^{4}\alpha, \\ \cos^{5}\alpha, \cos^{6}\alpha\end{pmatrix} \quad (27)$$

M^{max} shows the maximum cosine similarity value of parameters d_1 and d_2, d_1 and d_3, d_1 and d_4, d_2 and d_3, d_2 and d_4, d_3 and d_4.

- The average of the four different positions of the five neighboring pixels of the central pixel are calculated based on figure 4 (N=5) and then we go to step 5 (N=5).

$$x_{avg}^{1} = \frac{1}{N}\sum(x_{i-1,j-1}, x_{i-1,j}, x_{i-1,j+1}, x_{i,j-1}, x_{i,j+1}) \quad (28)$$

$$x_{avg}^{2} = \frac{1}{N}\sum(x_{i,j-1}, x_{i+1,j-1}, x_{i+1,j}, x_{i+1,j+1}, x_{i,j+1}) \quad (29)$$

$$x_{avg}^{3} = \frac{1}{N}\sum(x_{i-1,j}, x_{i-1,j+1}, x_{i,j+1}, x_{i+1,j+1}, x_{i+1,j}) \quad (30)$$

$$x_{avg}^{4} = \frac{1}{N}\sum(x_{i-1,j-1}, x_{i-1,j}, x_{i,j-1}, x_{i+1,j-1}, x_{i+1,j}) \quad (31)$$

$$x_{avg}^{Max} = (x_{avg}^{1}, x_{avg}^{2}, x_{avg}^{3}, x_{avg}^{4}) \quad (32)$$

- Train the ANFIS structure for a maximum of 30 epochs. Stop training if the error value computed by using the output value of ANFIS is less than 0.001. Restore the gray value $x_{i,j}$ of the corrupted pixel.

M^{max}, x_{avg}^{Max} and the noise pixel value are considered the three inputs of anfis. The original image is the output of anfis. Since Anfis receives noisy pixels as input, it replaces the noisy pixel with a value closer to the original image's pixel.

In the Anfis structure used for two inputs, M^{max},x_{avg}^{Max} each has five membership functions, and the third input has three triangular membership functions. The output membership function is considered linear, and the number of rules is 75.

6. Experimental results

This section discusses different results of the method proposed in this article. Algorithms presented in the proposed method have been tested on 698 images such as Barbara, Airplane, Cameraman, Baboon, Parrot, Boat, House, Lena, Man, and Monarch with dimensions of 512 × 512 pixels. Figure 5 shows an example of these images.

Performance of proposed method compared with other conventional and state of the art methods such as ($SMMF^1$ and $SMMF^2$ [36]) with the existing methods which are ASMF [13], LMMF [19], IMF [18] and DNLM [17] and proposed method.

Fig. 5. An example of test images Barbara, Airplane, Cameraman, Baboon, Parrot, Boat, House, Lena, Man, and Monarch from 830 test images.

Table.1.
Comparison of various filtering for the Lena

Methods	*Noise Ratio*						
	10%	*20%*	*30%*	*40%*	*50%*	*60%*	*70%*
IMF	39.2	34.3	32.1	30.2	28.5	27.0	25.9
LMMF	42.9	38.8	36.8	34.8	32.7	31.0	29.0
DNLM	41.9	38.7	36.7	34.8	32.5	29.8	27.4
ASMF	45.3	41.2	38.4	36.6	34.9	33.3	31.8
$SMMF^1$	45.5	41.5	39.6	38.0	36.5	35.0	33.4
$SMMF^2$	46.2	42.5	40.6	38.5	36.8	35.3	33.5
Proposed	47.2	43.2	41.1	39.2	37.6	36.2	34.3

Table.2.
Comparison of various filtering for the Barbara

Methods	*Noise Ratio*						
	10%	*20%*	*30%*	*40%*	*50%*	*60%*	*70%*
IMF	24.5	23.9	23.2	23.1	22.9	22.7	22.1
LMMF	33.1	29.0	27.0	25.4	24.4	23.1	22.5
DNLM	33.6	30.6	28.4	27.3	25.9	24.9	23.6
ASMF	33.5	30.4	28.3	26.9	25.6	24.5	23.5
$SMMF^1$	34.0	31.1	29.0	27.5	26.4	25.4	24.6
$SMMF^2$	34.1	30.8	29.0	27.6	26.4	25.4	24.4
Proposed	35.5	31.7	30.0	28.0	27.1	26.1	25.1

Table.3.
Comparison of various filtering Peppers

Methods	*Noise Ratio*						
	10%	*20%*	*30%*	*40%*	*50%*	*60%*	*70%*
IMF	31.3	30.0	28.3	28.0	27.9	26.6	25.1
LMMF	40.8	37.7	35.5	33.8	32.1	30.9	29.2
DNLM	39.9	36.8	35.1	33.3	31.5	29.1	26.6
ASMF	41.7	38.3	36.4	34.4	32.9	31.1	30.0
$SMMF^1$	41.8	38.3	36.5	34.8	33.6	32.3	31.1
$SMMF^2$	42.8	39.2	37.0	35.3	33.8	32.4	30.9
Proposed	43.0	40.1	38.1	36.1	34.2	33.1	31.2

Also, the performance and quality of the presented restoration compared to other methods are measured and evaluated with the following measures PSNR and SSIN [34–38]:

$$PSNR = 10log_{10}\left(\frac{255^2}{MSE}\right) \quad (33)$$

Where 255 is the maximum pixel intensity for 8-bit gray scale images, MSE is the mean square error, which is inserted between the original and restored images, which is calculated by Eq (34):

$$MSE = \frac{1}{m*n}\sum_{i=1}^{m}\sum_{j=1}^{n}(O_{ij} - R_{ij})^2 \quad (34)$$

"O" is the original image (o_{ij} pixel of the original image) and R is the restored image (R_{ij} pixel of the "restored image). Also, "m" and "n" are the width and height of the image.

The structural similarity index measure (SSIM) between the original image and the restored image is calculated as follows:

$$\text{SSIM} = \frac{(2\mu_O\mu_R+c_1)(2\sigma_{OR}+c_2)}{(\mu_O^2+\mu_R^2+c_1)(\sigma_O^2+\sigma_R^2+c_2)} \quad (35)$$

Where, $\sigma_O = \sqrt{\frac{1}{n-1}\sum_{i=1}^{n}(O_i - \mu_O)^2}$ and $\mu_O = \frac{1}{n}\sum_{i=1}^{n} O_i$ are the variance and average of original image, $\sigma_R = \sqrt{\frac{1}{n-1}\sum_{i=1}^{n}(R_i - \mu_R)^2}$ and $\mu_R = \frac{1}{n}\sum_{i=1}^{n} R_i$ are the variance and average of restored image. $\sigma_{OR} = \sqrt{\frac{1}{n-1}\sum_{i=1}^{n}(O_i - \mu_O)(R_i - \mu_R)}$ is the covariance of original and restored image. L is the dynamic range of the pixel values that for an 8-bit grayscale image composed of 0-255 gray-levels, $c_1 = (k_1 L)^2$ and $c_2 = (k_2 L)^2$, where $k_1 \ll 1$ and $k_2 \ll 1$ are small constants [1-2, 32].

Tables 1-3 show the results of PSNR values for different methods and the method proposed in this article. The proposed method has obtained the highest PSNR values compared to the other methods for Lena, Barbara, and Pepper images degraded by impact noise. Also, the IMF, LMMF, and DNLM methods obtained lower values than the other methods for the images of Lena, Barbara, and Pepper. Figures 6-8 show the PSNR graph for different methods and the proposed method for Lena, Barbara, and Pepper images. These images are corrupted by 90% of the impulse noise, and the proposed method shows the best PSNR graph compared to other methods. In fact, compared to other methods, the proposed method has removed the noise from the target images better and restored the target images well. Also, Table 4 shows the SSIM values of different methods for the Lena, Barbara, and Pepper images. This table shows that the proposed method has obtained the best results compared to other methods.

Table.4.
Comparison of the SSIM values for Lena and Barbara and Peppers

Methods	*Lena SSIM*	*Barbara SSIM*	*Peppers SSIM*
IMF	0.54	0.49	0.51
LMMF	0.52	0.46	0.49
DNLM	0.56	0.44	0.53
ASMF	0.57	0.47	0.54
$SMMF^1$	0.61	0.54	0.59
$SMMF^2$	0.63	0.55	0.61
Proposed	0.65	0.59	0.63

Figures. 9 shows the restored results of all the evaluated filters for the Lena and Barbara image corrupted by 70% density impulse noise, respectively. As can be seen in these figures, the method proposed in this article removed the impact noise better than the other methods in the images of Lena and Barbara. Also, these results show that the proposed method has restored these images well by preserving image details such as edges.

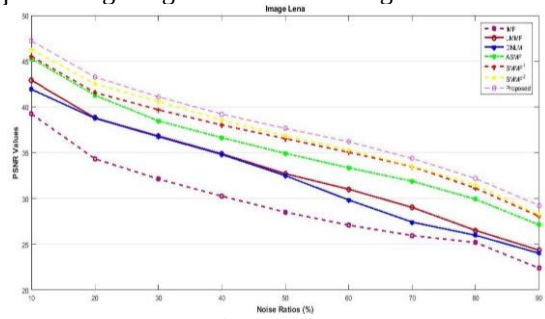

Fig. 6. Comparison of PSNR values on Lena restored image by 10% to 90% impulse noise.

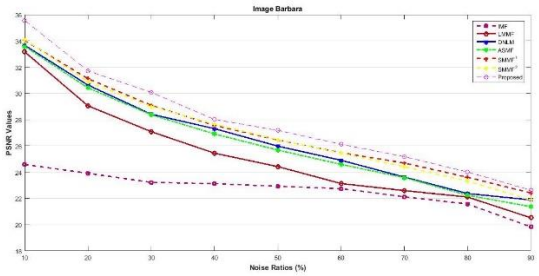

Fig. 7. Comparison of PSNR values on Barbara restored image by 10% to 90% impulse noise.

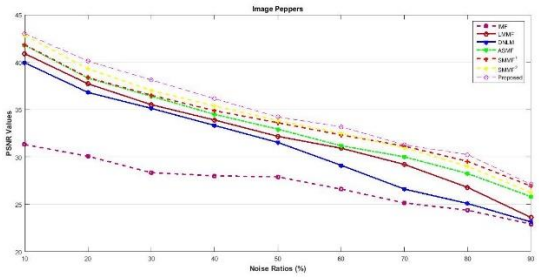

Fig. 8. Comparison of PSNR values on Peppers restored image by 10% to 90% impulse noise.

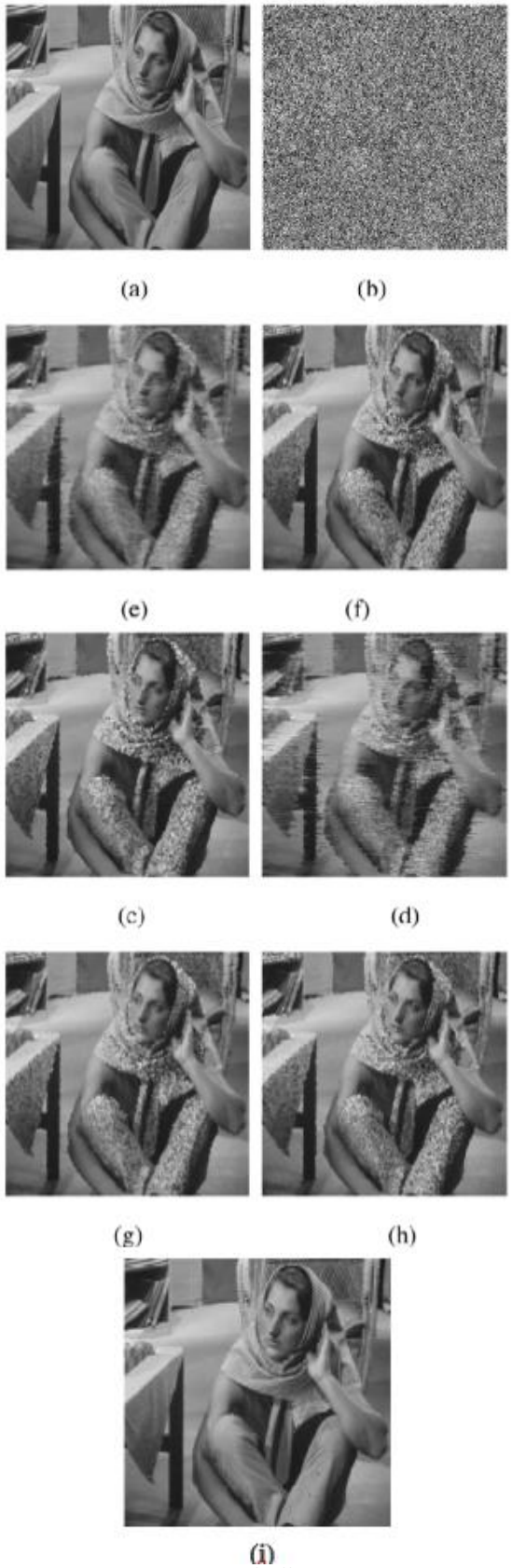

Fig. 9. Restoration results of different methods in restoring corrupted Barbara image: (a) original noise-free image, (b) 70% noise corrupted, (c) IMF, (d) LMMF, (e) DNLM,(f) ASMF, (g) $SMMF^1$, (h) $SMMF^2$ and (i) proposed method.

The feature of the method presented in this article is its simplicity, robustness and parallelism compared to other methods, which effectively and efficiently preserves meaningful details in the image and identifies noisy pixels in the image in two separate phases, and retrieves the image.

7. Conclusion

This article proposes an innovative method that includes three new algorithms to remove impact noise from digital images. These new algorithms, by two phases proposed in this paper, identify the impulse noise pixels in the image and restore the image. One of the advantages of the proposed method related to the first phase is that the identification and detection of corrupted pixels in the image are made in two steps, which results in better performance in identifying the damaged pixels of the image. The restored results show that the proposed method performs better than other methods in terms of PSNR and SSIM, and the details of the restored images, such as edges, are well preserved. Other advantages of the proposed method are noise robustness and parallelism to restore a wide range of images (10-90%) corrupted by impulse noise.

References

[1] M.M.Piroozmandan, F.Farokhi, K.Kangarloo, M.Jahanshahi," Removing High Density Impulse Noise via a Novel Two Phase Method Using Fuzzy Cellular Automata", International Journal of Smart Electrical Engineering, (2021) 177 - 186.

[2] M.M.Piroozmandan, F.Farokhi, K.Kangarloo, M.Jahanshahi," Removing the impulse noise from images based on fuzzy cellular automata by using a two-phase innovative method" ,Optik –International Journal for Light and Electron Optics , (2022) 168-713., https://doi.org/10.1016/j.ijleo.2022.168713.

[3] W. Zhang, L. Jin , E. Song, X. Xu, "Removal of impulse noise in color images based on convolutional neural network", Applied Soft Computing Journal,(2019) 105-558. https://doi.org/10.1016/j.asoc.2019.105558.

[4] J. Zhang, "An efficient median filter based method for removing random-valued impulse noise", Digital Signal Process, (2010) 20:1010–8., https://doi.org/10.1016/j.dsp.2009.11.003.

[5] L. Yin, R. Yang, M. Gabbouj , Y. Neuvo , "Weighted median filters: a tutorial", IEEE Trans Circuits Syst II: Anal Digit Signal Process, (1996) 43:157–92.

[6] M.E. Celebi ,Y.A Aslandogan , "Robust switching vector median filter for impulsive noise removal", J Electronic Imaging, (2008) 17:043006–43011. https://doi.org/10.1117/1.2991415.

[7] V.R.V Kumar ,S. Manikandan ,P.T Vanathi, "Adaptive window length recursive weighted median filter for removing impulse noise in images with details preservation", Ecti Trans Elec Eng Electron Commun, (2008) 6:73–80.

[8] S. Akkoul, R. Ledee, R. Leconge, R. Harba, "A new adaptive switching median filter", IEEE Signal Process Lett, (2010) 17:587–90.

[9] S.J. Ko, Y.H. Lee, "Center weighted median filters and their applications to image enhancement", IEEE Trans. Circuits Syst. 38 (9) (1991) 984–993.

[10] H. Hwang, R.A. Haddad, "Adaptive median filters: new algorithms and results", IEEE Trans. Image Process. 4 (4) (1995) 499–502.

[11] T. Chen, H.R. Wu, "Adaptive impulse detection using center weighted median filters", IEEE Signal Process. Lett. 8 (1) (2001) 1–3.

[12] G.R. Arce, J.L. Paredes, "Recursive weighted median filters admitting negative weights and their optimization", IEEE Trans. Signal Process. 48 (3) (2000) 768–779.

[13] X. Wang, X.Q. Zhao, F.X. Guo, J.F. Ma, "Impulsive noise detection by double noise detector and removal using adaptive neural-fuzzy inference system", Int J. Electron Commun. (AEU) 65 (5) (2010) 429–439. https://doi.org/10.1016/j.aeue.2010.06.004.

[14] M.E. Yuksel, A. Bastrk, "Efficient removal of impulse noise from highly corrupted digital images by a simple neuro-fuzzy operator", AEU Int. J. Electron. Commun. 57 (3) (2003) 214–219. https://doi.org/10.1078/1434-8411-54100164.

[15] M.T. Yildirim, A. Basturk, M.E. Yuksel, "Impulse noise removal from digital images by a detail-preserving filter based on type-2 fuzzy logic", IEEE Trans. Fuzzy Syst. 16 (4) (2008) 920–928, 920–228.

[16] K.K.V. Toh , I. NAM , Noise adaptive fuzzy switching median filter for salt-and-pepper noise reduction. IEEE Sig Process Lett , (2010) 17(3):281–4 .

[17] V. Gregori, S. Morillas, B. Roig, Almanzor Sapena, "Fuzzy averaging filter for impulse noise reduction in color images with a correction step", J. Vis. Commun. Image Represent, (2018) 518–528. https://doi.org/10.1016/j.jvcir.2018.06.025.

[18] V.P. Ananthi, P. Balasubramaniam," A new image denoising method using interval-valued intuitionistic fuzzy sets for the removal of impulse noise", Signal Process, (2016) 81–93. https://doi.org/10.1016/j.sigpro.2015.10.030.

[19] S. Ulam," Some ideas and prospects in biomathematics", Annu. Rev. Biophys. Bioeng. 1 (1972) 277–292.

[20] J.V. Neumann, "Theory of Self-Reproducing Automata", University of Illinois Press, 1966, pp. 63–87.

[21] S. Wolfram, "Computation theory of cellular automata, Commun". Math. Phys. 96 (1984) 15–57.

[22] U. Sahin, S. Uguz, F. Sahin, Salt and pepper noise filtering with fuzzy-cellular automata, Comput. Electr. Eng. 40 (1) (2014) 59–69. https://doi.org/10.1016/j.compeleceng.2013.11.010.

[23] G. Cattaneo, P. Flocchini, G. Mauri, C.Q. Vogliotti, N. Santoro, "Cellular automata in fuzzy backgrounds, Phys. D Nonlinear Phenom", 105 (1–3) (1997) 105–120. https://doi.org/10.1016/S0167-2789(96)00233-3.

[24] P.L. Rosin, "Image processing using 3-state cellular automata", Comput. Vis. Image Underst. 114 (7) (2010) 790–802. https://doi.org/10.1016/j.cviu.2010.02.005.

[25] S. Sadeghi, A. Rezvanian, E. Kamrani, "An efficient method for impulse noise reduction from images using fuzzy cellular automata", AEU Int. J. Electron. Commun. 106 (9) (2012) 772–779. https://doi.org/10.1016/j.aeue.2012.01.010.

[26] E. Besdok, P. Civicioglu, M. Alci, "Using an adaptive neuro-fuzzy inference system based interplant for impulsive noise suppression from highly distorted images", Fuzzy Sets Syst (2005) 150:525–43.

[27] J. Jang, "Anfis: adaptive-network-based fuzzy inference system", IEEE Trans Systems Man Cybern (1993) 23:665–85.

[28] MathWorks: Matlab, fuzzy logic toolbox, user's guide. New York: The Math Works Inc.; (2002).

[29] T. Veerakumar, B.N. Subudhi, S.L. Esakkirajan, P.K. Pradhan, "Context model based edge preservation filter for impulse noise removal", Expert Syst. Appl, (2017) 29–44. https://doi.org/10.1016/j.eswa.2017.06.033.

[30] S. Schulte, W.V. De, M. Nachtegael, D.V.D. Weken, E.E. Kerre," Fuzzy random impulse noise reduction method", Fuzzy Sets Syst. 158 (3) (2007) 270–283. https://doi.org/10.1016/j.fss.2006.10.010.

[31] H. Deng, Q. Zhang, X. Song, J. Tao, "A decision-based modified total variation diffusion method for impulse noise removal", Hindawi Comput. Intell. Neurosci,(2017), 2024396.

[32] ZH. Wang, A.C. Bovik, H.R. Sheikh, E.P. Simoncelli, "Image quality assessment: from error visibility to structural similarity", IEEE Trans Image Process,2004.

[33] X. Li, T. sun, "Mixed Gaussian-impulse noise removal using non-convex high-order TV penalty", Applied Numerical Mathematics,(2024) 114614. https://doi.org/10.1016/j.cam.2022.114615.

[34] X. Zeng,R. Lv, S. Li, "The maximum a posteriori estimation model for signal recovery with mixed Gaussian and impulse noise", Applied Mathematics Letters,(2024), https://doi.org/10.1016/j.aml.2023.108859.

[35] R. Li, B. Zheng, "A spatially adaptive hybrid total variation model for image restoration under Gaussian plus impulse noise", Applied Mathematics and Computation,(2022), https://doi.org/10.1016/j.amc.2021.126862.

[36] CH. Zhang, K. Wang," A switching median–mean filter for removal of high-density impulse noise from digital images", Optik, (2015) 956–961, https://doi.org/10.1016/j.ijleo.2015.02.085.

[37] X. Liu, T. Sun," Mixed Gaussian-impulse noise removal using non-convex high-order TV penalty", Applied Numerical Mathematics,201 (2024) Pages 72-84, https://doi.org/10.1016/j.apnum.2024.02.012.

[38] C.J.J Sheela, G. Suganthi, "An efficient denoising of impulse noise from MRI using adaptive switching modified decision based unsymmetric trimmed median filter", Biomedical Signal Processing and Control, 55 (2020) Pages 101657 ,https://doi.org/10.1016/j.bspc.2019.101657.

[39] V. Gregori, S. Morillas, B. Roig, Almanzor Sapena, "Fuzzy averaging filter for impulse noise reduction in color images with a correction step", J. Vis. Commun. Image Represent. 55 (2018) 518–528. https://doi.org/10.1016/j.jvcir.2018.06.025.

[40] V.P. Ananthi, P. Balasubramaniam," A new image denoising method using interval-valued intuitionistic fuzzy sets for the removal of impulse noise", Signal Process. 121 (2016) 81–93. https://doi.org/10.1016/j.sigpro.2015.10.030

[41] N.U. Khan, K. V. Arya, "A new fuzzy rule based pixel organization scheme for optimal edge detection and impulse noise removal", Multimedia Tools and Applications, 79 (2020), https://doi.org/10.1007/s11042-020-08707-x.

[42] U. Erkan, L. Gökrem, S. Enginoglu, Different applied median filter in salt and pepper noise, Comput. Electr. Eng. 70 (2018) 789–798. http://dx.doi.org/10.1016/j.compeleceng.2018.01.019.

[43] K. Vasanth, R. Varatharajan, An adaptive content based closer proximity pixel replacement algorithm for high density salt and pepper noise removal in images, J. Ambient Intell. Humaniz. Comput. (2020) http://dx.doi.org/10.1007/s12652-020-02376-2.

[44] B. Karthik, T. Krishna Kumar, S.P. Vijayaragavan, M. Sriram, Removal of high density salt and pepper noise in color image through modified cascaded filter, J. Ambient Intell. Humaniz. Comput. 12 (3) (2021) 3901–3908, http://dx.doi.org/10.1007/s12652-020-01737-1.

[45] A. Roy, R.H. Laskar, Multiclass SVM based adaptive filter for removal of high density impulse noise from color images, Appl. Soft Comput. 46 (2016) 816–826, http://dx.doi.org/10.1016/j.asoc.2015.09.032.

[46] M. González-Hidalgo, S. Massanet, A. Mir, D. Ruiz-Aguilera, Improving salt and pepper noise removal using a fuzzy mathematical morphology-based filter, Appl. Soft Comput. 63 (2018) 167–180, http://dx.doi.org/10.1016/j.asoc.2017.11.030.

[47] S. Enginoğlu, U. Erkan, S. Memiş, Adaptive cesáro mean filter for saltand- pepper noise removal, El-Cezeri J. Sci. Eng. 7 (1) (2020) 304–314, http://dx.doi.org/10.31202/ecjse.646359.

[48] B. Garg, K.V. Arya, Four stage median-average filter for healing high density salt and pepper noise corrupted images, Multimedia Tools Appl. 79 (43) (2020) 32305–32329, http://dx.doi.org/10.1007/s11042-020-09557-3.